AD-A157 512 ANALYSIS AND INTERPRETATION OF THE SHOCK-LIKE ELECTROSTATIC NOISE OBSERVE. (U) IOWA UNIV IOWA CITY DEPT OF PHYSICS AND ASTRONOMY D A GURNETT ET AL. 1/1

UNCLASSIFIED MAY 85 U. OF IOWA-85-13 N00014-76-C-0016 F/G 3/2 NL

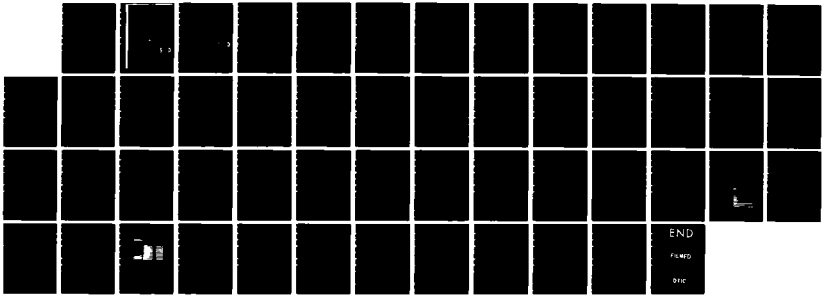

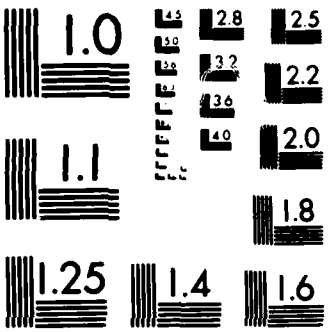

MICROCOPY RESOLUTION TEST CHART

ANALYSIS AND INTERPRETATION OF THE SHOCK-LIKE ELECTROSTATIC NOISE OBSERVED DURING THE AMPTE SOLAR WIND LITHIUM RELEASES

by

D. A. Gurnett[1], T. Z. Ma[1], R. R. Anderson[1],
O. H. Bauer[2], G. Haerendel[2], B. Häusler[2],
G. Paschmann[2], R. A. Treumann[2], H. C. Koons[3],

Department of Physics and Astronomy
THE UNIVERSITY OF IOWA
Iowa City, Iowa 52242

U. of Iowa 85-13

ANALYSIS AND INTERPRETATION OF THE SHOCK-LIKE ELECTROSTATIC NOISE OBSERVED DURING THE AMPTE SOLAR WIND LITHIUM RELEASES

by

D. A. Gurnett[1], T. Z. Ma[1], R. R. Anderson[1],
O. H. Bauer[2], G. Haerendel[2], B. Häusler[2],
G. Paschmann[2], R. A. Treumann[2], H. C. Koons[3],
R. Holzworth[4], and H. Lühr[5]

[1] Department of Physics and Astronomy, The University of Iowa, Iowa City, IA 52242

[2] Max-Planck-Institut für Physik und Astrophysik, Institut für extraterrestrische Physik, 8046 Garching, West Germany

[3] The Aerospace Corporation, P. O. Box 92957, Los Angeles, CA 90009

[4] Geophysics Program, University of Washington, Seattle, WA 98195

[5] Institut für Geophysik und Meteorologie Technische Universität Braunschweig, 3300 Braunschweig, West Germany

UNCLASSIFIED

SECURITY CLASSIFICATION OF THIS PAGE (When Data Entered)

REPORT DOCUMENTATION PAGE

READ INSTRUCTIONS BEFORE COMPLETING FORM

1. REPORT NUMBER: U. of Iowa 85-13

2. GOVT ACCESSION NO.: A157612

3. RECIPIENT'S CATALOG NUMBER:

4. TITLE (and Subtitle): ANALYSIS AND INTERPRETATION OF THE SHOCK-LIKE ELECTROSTATIC NOISE OBSERVED DURING THE AMPTE SOLAR WIND LITHIUM RELEASES

5. TYPE OF REPORT & PERIOD COVERED: Progress January 1985

6. PERFORMING ORG. REPORT NUMBER:

7. AUTHOR(s): D. A. Gurnett, T. Z. Ma, R. R. Anderson, O. H. Bauer, G. Haerendel, B. Hausler, G. Paschmann, R. A. Treumann, H. C. Koons, R. Holzworth, and H. Luhr

8. CONTRACT OR GRANT NUMBER(s): N00014-76-C-0016, N00014-82-K-0183

9. PERFORMING ORGANIZATION NAME AND ADDRESS:
Department of Physics and Astronomy
University of Iowa
Iowa City, IA 52242

10. PROGRAM ELEMENT, PROJECT, TASK AREA & WORK UNIT NUMBERS:

11. CONTROLLING OFFICE NAME AND ADDRESS:
Electronics Program Office
Office of Naval Research
Arlington, VA 22217

12. REPORT DATE: May 1985

13. NUMBER OF PAGES: 36

14. MONITORING AGENCY NAME & ADDRESS (if different from Controlling Office):

15. SECURITY CLASS. (of this report): UNCLASSIFIED

15a. DECLASSIFICATION/DOWNGRADING SCHEDULE:

16. DISTRIBUTION STATEMENT (of this Report)

Approved for public release; distribution is unlimited.

17. DISTRIBUTION STATEMENT (of the abstract entered in Block 20, if different from Report)

18. SUPPLEMENTARY NOTES

Submitted to J. Geophys. Res.

19. KEY WORDS (Continue on reverse side if necessary and identify by block number)

Lithium Releases
Electrostatic Noise
AMPTE
Solar Wind

20. ABSTRACT (Continue on reverse side if necessary and identify by block number)

(See following page)

Accession For	
NTIS GRA&I	X
DTIC TAB	☐
Unannounced	☐
Justification	
By	
Distribution/	
Availability Codes	
Dist	Avail and/or Special
A-1	

DD FORM 1 JAN 73 1473 EDITION OF 1 NOV 65 IS OBSOLETE
S/N 0102-LF-014-6601

UNCLASSIFIED

SECURITY CLASSIFICATION OF THIS PAGE (When Data Entered)

ABSTRACT

During the AMPTE (Active Magnetospheric Particle Tracer Explorers) solar wind lithium release on September 11, and again on September 20, 1984, an intense burst of electrostatic noise was observed near the upstream edge of the ion cloud. Comparisons with measurements by the IMP-6 and ISEE-1 spacecraft show that the spectrum and overall features of this noise are very similar to electrostatic noise observed at the earth's bow shock. A stability analysis using realistic parameters shows that the electrostatic noise can be accounted for by an ion beam-plasma instability caused by the solar wind proton beam streaming through the nearly stationary lithium cloud. The growth rate of this instability is largest when the ion density and solar wind proton density are similar, which explains why the noise only occurs near the outer edge of the ion cloud.

The similarity to the noise in the earth's bow shock suggests that a shock may exist in the solar wind plasma flow upstream of the ion cloud. If the noise is associated with a shock, then it must be an electrostatic shock, since the ion cyclotron radii are too small for the existence of a MHD shock. Since the electrostatic instability occurs at phase velocities near the lithium thermal velocity, the electrostatic turbulence may play a role in heating the lithium ions and transferring momentum from the solar wind to the ion cloud.

The noise may also play a role in the pitch-angle scattering and diffusion of energetic electrons observed in the vicinity of the ion cloud. Because of the similarity to the solar wind interaction with the gaseous envelope of a comet, it is expected that similar types of wave-particle effects may occur upstream of comets.

I. INTRODUCTION

On September 11 and again on September 20, 1984, a cloud of lithium gas was released in the solar wind upstream of the earth's bow shock as part of the AMPTE (Active Magnetospheric Tracer Explorers) program. Numerous effects were observed in the immediate vicinity of the releases, including (1) the creation of a dense rapidly expanding cloud of ionized lithium, (2) the formation of a diamagnetic cavity, and (3) the occurrence of an intense shock-like burst of electrostatic noise in the region upstream of the cavity. A summary of these effects is given in an accompanying paper by Haerendel et al. [1985]. The purpose of this paper is to present a detailed analysis of the shock-like electrostatic noise and to investigate the origin of this noise. Comparisons are also made with a similar type of noise observed in the earth's bow shock.

The primary objective of the AMPTE program is to use artificially injected barium and lithium ions as tracers to study the transport and energization of charged particles in the earth's magnetosphere, and a secondary objective is to study the physics of the injection process [Krimigis et al., 1982]. Three spacecraft are involved in the project: the Ion Release Module (IRM) which carries the barium and lithium canisters, the United Kingdom Subsatellite (UKS) which orbits near the IRM to study the expansion and evolution

of the ion cloud, and the Charge Composition Explorer (CCE) which searches for the tracer ions in the inner regions of the magnetosphere.

The data presented in this paper are from the plasma wave experiment on the IRM. The IRM is in a low-inclination highly eccentric orbit with an apogee geocentric radial distance of 19.0 R_E. During the September 1984 releases, the apogee was on the dayside of the earth near local noon. The ion cloud is produced by releasing two canisters containing lithium or barium in diametrically opposite directions from the IRM. Ten minutes after the release the two canisters are exploded simultaneously at a distance of about 1 km from the spacecraft. The atoms vaporized by the explosion then form an expanding cloud of neutral gas which sweeps over the spacecraft a few seconds after the explosion. Ultraviolet radiation from the sun subsequently ionizes the neutral gas, thereby producing a cloud of ionized gas. For a discussion of the physics of the ion cloud formation and expansion, see Haerendel [1983, 1985].

A variety of particle and field instruments on the IRM are used to analyze the plasma effects associated with the ionized gas cloud. For a list of these instruments and their characteristics, see Krimigis et al. [1982]. The measurements of particular interest for this paper are from the plasma wave instrument. The plasma wave instrument uses a 47m tip-to-tip electric dipole antenna for electric field measurements and two search coil antennas for magnetic field

measurements. The signals from the electric and magnetic antennas are processed by a variety of receivers and spectrum analyzers provided by three groups: the University of Iowa, the Max-Planck-Institut, and the Aerospace Corporation. For a complete description of this instrumentation, see Häusler et al. [1985a].

II. CHARACTERISTICS OF THE INTENSE ELECTROSTATIC NOISE

The overall features of the plasma wave observations are very similar for both the September 11th and September 20th lithium releases. Since a survey of the plasma wave observations is given in a companion paper by Häusler et al. [1985b], we will not repeat the detailed description of both events. For purposes of analyzing the origin of the intense electrostatic noise it is sufficient to use the September 20th event as a model. The plasma interactions during this event tend to be the least complicated and most readily amenable to a theoretical analysis.

A summary of the plasma density, magnetic field and plasma wave electric field data obtained during the September 20th event is shown in Figure 1. The top panel shows the plasma density obtained from an analysis of electron plasma oscillations observed by the plasma wave instrument [Anderson et al., 1985], the second panel shows the magnetic field from the magnetometer [Lühr et al., 1985], the third panel shows the electric field spectrum from the wideband receiver, and the bottom panel shows the electric field intensities from the 16-channel plasma wave spectrum analyzer. The canisters of lithium were exploded at 0956:02 UT, near the left edge of the plot. About 0.2 seconds after the injection the plasma density jumps up to about 10^5 cm^{-3}, the magnetic field drops to near zero, and an impulsive

disturbance occurs in the low frequency electric field channels. These effects mark the arrival of the lithium ion cloud. The depressed magnetic field indicates that the spacecraft is in the diamagnetic cavity formed by the dense ion cloud. The geometry of this cavity is illustrated in Figure 2. As the lithium ion cloud expands the plasma density decreases. The cloud also starts to move downstream, away from the sun, because of stresses imposed by the solar wind. About 7 seconds after the explosion the magnetic field begins to increase. At this time the cloud has moved downstream to the point where the spacecraft is passing through the sunward boundary of the diamagnetic cavity. The spacecraft then enters a region of enhanced plasma density and strong magnetic field. The peak strength of the magnetic field is about six times stronger than the ambient solar wind magnetic field. This region of compressed plasma and strong magnetic field is caused by the "pileup" of plasma around the nose of the cloud due to the interaction with the solar wind. The magnetic field is believed to be draped around the diamagnetic cavity as shown in Figure 2.

As the ion cloud moves farther downstream, a region of very intense electric field noise is encountered about 17 seconds after the injection. This region of intense electric field noise is located on the sunward side of the compression region, in a region where the magnetic field is returning to the pre-event value. The region of intense electric field noise also appears to coincide with a brief increase in the plasma density. Because considerable uncertainty exists about the precise shape of the plasma density profile

in this region (see Anderson et al. [1985]), this portion of the plasma density profile is shown by dashed lines in Figure 2. The intense electric field noise continues for about 10 seconds, slowly decreasing in intensity as the magnetic field returns to the upstream value.

At no time during the event was any noise comparable to that shown in Figure 1 detected with the search coil magnetometers. The absence of a comparable magnetic component indicates that the noise is electrostatic, which is not surprising since no electromagnetic mode exists in the frequency range where the noise is observed (between the electron cyclotron frequency and the electron plasma frequency). The spectrum of the electrostatic noise is shown in Figure 3. Two types of spectrums are shown, labelled peak and average. The peak is the maximum electric field spectral density observed over a 1.0 second interval and the average is the electric field spectral density averaged over a 50 msec interval. The time for the spectrums shown in Figure 3 is 0956:19.53 UT, which is near the point of maximum intensity. The peak and average broadband field strengths, integrated from 31 Hz to 178 kHz, are 40.4 and 6.6 mVm^{-1}, respectively. These intensities are among the most intense ever recorded by a space plasma wave experiment.

The noise in Figure 3 is characterized by a very broad peak extending from a few tens of Hz up to a few hundred kHz. Above a few kHz the intensity drops very rapidly, to near the instrument noise

level at frequencies above about 10 kHz. The peak spectrum shows a broad maximum at a frequency of about 178 Hz, and the average spectrum shows a discontinuity in the slope at about 1.78 kHz. These detailed features are probably not significant, since they vary somewhat from event to event. For example, the corresponding average spectrum for the September 11th event, shown in Figure 4, does not show a discontinuity in the slope. Also, the average spectrum for the September 11th event shows a peak at about 178 Hz, whereas the average spectrum for the September 20th event decreases monotonically over the entire frequency range measured.

High resolution wideband spectrums, such as in the third panel of Figure 1, show that the noise tends to be somewhat impulsive, consisting of many short bursts lasting only a fraction of a second. This impulsive character accounts for the large difference between the peak and average spectrums in Figure 3. The impulsive character of the noise also varies somewhat from event to event. The September 11th event in Figure 4 has a smaller difference between the peak and average intensities, which shows that the noise was less impulsive during this event. No evidence for spin modulation is evident in the electric field intensities, which indicates that the electric field, hence wave vector direction, tends to be distributed over a broad range of angles.

V. CONCLUSION

We have presented a detailed analysis of the shock-like electrostatic noise observed upstream of the AMPTE artificial ion clouds and have described an ion beam-plasma instability that can account for the main features of this noise. Comparisons with other spacecraft measurements show that this noise is very similar to the electrostatic noise observed in the earth's bow shock. This similarity suggests that a shock may be present in the solar wind flow upstream of the ion cloud. The available data do not confirm the existence of a shock, but also do not rule out the possibility. If the noise is associated with a shock, then the shock cannot be a MHD shock since the ion cyclotron radii are large compared to the radius of curvature of the discontinuity. The most likely possibility is that the noise is associated with an electrostatic shock. This possibility is supported by the fact that laboratory experiments [Ikezi et al., 1973] demonstrate that turbulent electrostatic shocks can be produced by injecting an ion beam into a plasma at rest, a physical situation qualitatively similar to injecting an ion cloud into the supersonically flowing solar wind.

An investigation of the instabilities caused by a solar wind proton beam streaming through a nearly stationary lithium ion cloud shows that the basic features of the electrostatic noise can be accounted for by an electrostatic ion beam-plasma instability. Using

shift the electron drift velocity relative to that given by Equation 2, which assumes zero current. Using representative values for the magnetic field variation, $\Delta B \simeq 35$ nT, and scale size, $\Delta L \simeq 200$ km, of the magnetic field structure, the current density is estimated to be 0.14 μAm^{-2}. For an electron density of 8 cm^{-3}, this current produces a shift in the electron drift velocity of about 25%. This shift is an upper limit, since in the more dense region of the cloud the shift required to produce the required current is smaller. Figure 13 shows the effect of a ±25% shift in the electron drift velocity for the case $N_e^c = N_{Li}$. Somewhat similar results are obtained for the case $N_e^c = 0$. As can be seen, a positive shift in the drift velocity (toward V_{sw}) increases the size of the unstable region, and a negative shift decreases the size of the unstable region. Generally, the effect of the current is quite small. Therefore, the basic instability is an ion beam-driven instability and not a current-driven instability. The currents that exist in the upstream boundary region are simply too small to play a major role in the stability considerations.

Although the cold electron temperature does not have a major effect on the instability boundaries, it does affect the growth rate somewhat. The maximum growth rate is shown in Figure 12 as a function of the density ratio N_{Li}/N_p. The solid line is for the case $N_e^c = 0$, and the dashed line is for the case $N_e^c = N_{Li}$. As can be seen the growth rate increases when the cold electrons are present. This dependence apparently occurs because the Landau damping decreases as the electron temperature decreases, which causes higher growth rates.

It can be easily shown that the growth rates in Figure 12, typically 25 to 75 sec^{-1}, are more than adequate to produce the observed intensities. From Figure 9 the group velocity, $\partial\omega/\partial k$ is estimated to range from about 5.3 to 50 km/sec. Taking a representative group velocity of 50 km/sec and a path length of 30 km a wave packet would propagate through the unstable region in 0.6 sec. For a representative growth rate of 25 sec^{-1}, the wave amplitude would grow by a factor of e^{15}. Waves of lower group velocity grow to even larger amplitudes. These simple estimates show that in a very short time the waves should grow to very large amplitudes. Although the detailed shapes of the spectrums in Figures 3 and 4 are controlled by nonlinear effects, the basic frequency range where the noise occurs appears to be accounted for by this linear stability analysis.

We now return to the zero current assumption. It is evident from the magnetic field variations that finite currents exist in the region where the noise occurs. The main effect of a current is to

A representative growth rate computation for the instability between 0 and V_D is shown in Figure 9. The bottom panel shows the growth rate, γ, plotted as a function of frequency, and the top panel shows the wave number, $k\lambda_D$, normalized by the Debye length, plotted as a function of frequency. The lithium and proton density are assumed to be equal, which represents the most unstable condition. The solid curve gives the case where $N_e^c = 0$, and the dashed curve gives the case where $N_e^c = N_{Li}$. Both cases give large growth rates, 25 sec^{-1} and 72 sec^{-1}, over a broad range of frequencies, up to about 250 Hz. This range of frequencies is in good agreement with the spectrums in Figures 3 and 4, which show that the most intense noise occurs at frequencies from a few tens of Hz up to a few hundred Hz.

Because the relative densities of the lithium ions and protons vary over a large range, it is useful to investigate the instability as a function of the lithium to proton density ratio, N_{Li}/N_p. Figures 10 and 11 show the frequency of marginal stability ($\gamma = 0$) as a function of the density ratio, N_{Li}/N_p. The dashed line labelled γ_{max} gives the frequency of maximum growth rate. Figure 10 is for the case $N_e^c = 0$, and Figure 11 is for the case $N_e^c = N_{Li}$. In both cases the instability occurs over a broad region, which shows that the basic mechanism is relatively insensitive to the assumed parameters. Figures 10 and 11 also confirm the previously mentioned fact that the instability only occurs over a limit range of lithium to proton density ratios. If the lithium to proton density ratio is less than about 2.5×10^{-2} the instability ceases, and if the ratio is above about 50 the the instability again ceases.

dispersion function [Fried and Conte, 1961]. The parameter z_s is a dimensionless quantity given by

$$z_s = \sqrt{\frac{m_s}{2\kappa T_s}} \left(\frac{\omega}{k} + i\frac{\gamma}{k}\right) \quad , \tag{4}$$

where m_s is the mass of the sth component and κ is Boltzmann's constant. The dispersion relation has been solved numerically for ω and γ using the Muller method [Muller, 1956]. Since it is not known whether a cold electron component is in fact present, the dispersion relation was analyzed for two extreme cases. First, it was assumed that $N_e^c = N_{Li}$. This case represents the situation where cold electrons associated with the lithium photoionization are still bound to the ion cloud. Second, it was assumed that $N_e^c = 0$. This amounts to assuming that all of the photoelectrons have escaped from the cloud and that no cold electrons are present.

Of the two instabilities discussed earlier, the growth rate computations show that the instability with phase velocities between 0 and V_D is the most important. The reason is that the lithium ion temperature, $T_{Li} = 2 \times 10^3$°K, is much lower than the proton temperature, $T_p = 1 \times 10^5$°K, which makes the double-hump associated with the lithium ions and electrons much more pronounced than the double hump associated with the electrons and protons. The instability with phase velocities between V_D and V_{sw} only occurs for proton temperatures less than about 3×10^4°K. Since the measured proton temperature is 1×10^5°K, this instability never occurs.

ambipolar electric field eventually disappears and the photoelectrons escape. The photoelectron density is then zero, $N_e^c = 0$. Macroscopic charge neutrality then implies that $N_e^h = N_p + N_{Li}$. Finally, we must consider the electron drift velocity. As a first approximation the $\vec{E} \times \vec{B}$ drift velocity can be estimated by assuming that the net current in the plasma is zero. Later we will consider the effect of a finite current. Using the condition for macroscopic charge neutrality, the zero current condition gives

$$V_d = \frac{N_p}{N_p + N_{Li}} V_{sw} \quad . \tag{2}$$

During the early dense phase of the ion cloud expansion, where $N_{Li} >> N_p$, the electron drift velocity is near zero, and during the later tenuous phase, where $N_{Li} << N_p$, the electron drift velocity is near the solar wind velocity.

Using the above parameters, the frequency ω and growth rate γ of electrostatic waves can be calculated from the electrostatic dispersion relation, which for a Maxwellian distribution is

$$D(\omega,\gamma) = 1 + \sum_s \frac{1}{(k\lambda_{Ds})^2} [1 + z_s Z(z_s)] = 0 \quad , \tag{3}$$

where the summation is over all components (s), k is the wave number, λ_{Ds} is the Debye length of the sth component, and Z is the plasma

proton densities, N_{Li} and N_p, which are shown in Figure 1, (4) the solar wind proton temperature, T_p, which is about 10^5°K [Coates et al., 1985], and (5) the hot electron temperature, T_e^h, which at energies above about 50 eV is about 5×10^5°K [Paschmann et al., 1985]. Parameters that are unknown because they cannot be measured by the plasma instrument are (1) the lithium ion temperature, T_{Li}, (2) the cold (photoelectron) temperature, T_e^c, and density N_e^c, and (3) the drift velocity of the electrons, V_d.

To proceed further suitable choices must be made for the unknown parameters. It is believed that the chemical reaction responsible for vaporizing the lithium yields a temperature of about 2×10^3°K [Haerendel et al., 1985]. Although the lithium ions could be colder due to time-of-flight effects, we will adopt the value, $T_{Li} = 2 \times 10^3$°K, for the lithium ion temperature. Since nothing is known about the photoelectrons associated with the lithium ionization, the best that can be done is to consider two extreme situations. During the early phase of the ion cloud expansion it is likely that the photoelectrons are bound to the ion cloud by the ambipolar electric field. In this case the cold electron density is equal to the lithium ion density, $N_e^c = N_{Li}$. Macroscopic charge neutrality then implies that $N_e^h = N_p$. Since the photoelectrons are ejected from the lithium ions with an energy distribution comparable to the characteristic energy of the solar ultraviolet spectrum (~ 1 eV) it is likely that the cold electron temperature is about 10^4°K. We will adopt the value $T_e^c = 10^4$°K. During the later phase of the ion cloud expansion the

small, V_d is expected to lie between the drift velocities of the lithium ions and the solar wind protons, as illustrated in Figure 8. The reduced distribution function then has two double humps, one associated with the lithium ions and electrons, and the other associated with the electrons and solar wind protons. Two instabilities are then expected, one with phase velocities $0 < \omega/k < V_d$, and the other with phase velocities $V_d < \omega/k < V_{sw}$. These instabilities only occur if the lithium ion and solar wind proton densities are somewhat comparable. Otherwise, the double hump associated with the minority ion disappears because the "beam" density is too low, and the double-hump associated with the majority ion disappears because the electrons drift at essentially the same velocity as the majority ion. These basic facts provide a simple explanation for why the noise only occurs near the outer boundary of the ion cloud. It is only in this region that the lithium ion and solar wind proton densities are comparable (see Figure 1).

To perform a detailed stability analysis we assume that the plasma distribution function consists of four Maxwellian components representing the lithium ions, the solar wind protons, the "hot" solar wind electrons, and the "cold" lithium photoelectrons. Each component is characterized by a density, a temperature, and a drift velocity. For the September 20th event the parameters that are reasonably well known are (1) the lithium drift velocity, which is essentially zero, (2) the solar wind velocity, V_{sw}, which is about 460 km/sec [Paschmann et al., 1985], (3) the lithium and solar wind

interaction, first analyzed in detail by Fried and Wong [1966]. For a further discussion of the ion beam-plasma instability, see Imre and Özizmir [1974].

It can be easily shown that the growth rate of electrostatic instabilities in an unmagnetized plasma is determined by a reduced (one-dimensional) distribution function, F(v), which is the sum of the electron (e) and ion (i) distribution functions,

$$F(v) = F_e + \sum_i \frac{m_e}{m_i} F_i(v) \quad , \tag{1}$$

where the ion terms $F_i(v)$ have weighting factors given by the electron to ion mass ratio, m_e/m_i. The plasma is unstable when the reduced distribution function is sufficiently double-humped to satisfy the Penrose criterion [Krall and Trivelpiece, 1973]. Because the electron to ion mass ratio is always very small, the ion terms must be sharply peaked and well separated for instability to occur. Because the thermal velocities of both the lithium ions and the solar wind protons are much smaller than the solar wind velocity, the distribution functions tend to satisfy this condition. However, it is also necessary to consider the role of the electrons. The electron distribution is expected to consist of two components: a "cold" component associated with the lithium photoionization, and a "hot" component associated with the solar wind electrons. Because the cyclotron radius of the electrons is small compared to the diameter of the cloud, both components are expected to drift at the $\vec{E} \times \vec{B}$ drift velocity, V_d. As long as the current is reasonably

IV. ORIGIN OF THE ELECTROSTATIC NOISE

Since the solar wind protons stream almost uninhibited through the ion cloud, it is evident that an ion beam-plasma instability may be a good candidate for producing the electrostatic noise. This instability would then be similar to the mechanism responsible for the electrostatic noise in the earth's bow shock. For super-critical shocks, such as in Figure 5, the electrostatic noise is closely correlated with the onset of ions (N_I) reflected from the bow shock [Gurnett, 1985]. These reflected ions produce an ion beam-plasma interaction that is very similar to the interaction that occurs as the solar wind protons stream through a stationary ion cloud.

Before we consider a quantitative analysis of the ion beam-plasma instability it is useful to discuss the qualitative aspects of this instability. The ion distribution function in the vicinity of the ion cloud is illustrated schematically in Figure 7. The lithium ions have a drift velocity near zero since they are born essentially at rest in the spacecraft frame of reference. The solar wind protons drift at a velocity corresponding to the upstream solar wind velocity, V_{sw}. The relative density of the lithium ions and solar wind protons varies with position in the ion cloud. Far upstream of the cloud the solar wind protons dominate, and in the dense central region of the cloud the lithium ions dominate. The double ion distribution in Figure 7 corresponds to the classical ion beam-plasma

cyclotron radius of a solar wind proton is 56 km. Lithium ions injected into the solar wind at a relative velocity of 400 km/sec have an even larger cyclotron radius, up to 2,500 km. Since these ion cyclotron radii are larger than the scale size of the ion cloud, the upstream disturbance cannot be a MHD shock.

If the disturbance is not a MHD shock then the only remaining possibility is that it is an electrostatic shock. Electrostatic shocks are characterized by a jump in the electrostatic potential on a spatial scale small compared to the ion cyclotron radii. Because the characteristic thickness of an electrostatic shock can be as small as a few Debye lengths, which is only about one hundred meters in the solar wind, an electrostatic shock could in principle occur upstream of the artificial ion cloud. Electrostatic shocks have received extensive theoretical study [Montgomery and Joyce, 1969; Forslund and Shonk, 1970; Tidman and Krall, 1971] and have been produced in laboratory plasmas [Ikezi et al., 1973; Means et al., 1973]. Both laminar and turbulent electrostatic shocks have been observed. Turbulent shocks are mainly associated with high Mach numbers, in which case the turbulence is produced by ions reflected from the electrostatic potential barrier at the shock. If the electrostatic noise observed upstream of the artificial ion cloud is caused by an electrostatic shock, it is almost certainly a turbulent shock, since the Mach number of the solar wind flow (8 to 10) is quite high.

shows that the solar wind protons stream through the ion cloud. Second, the solar wind velocity must decrease as the plasma flows across the discontinuity. This condition also appears to be satisfied. For the September 20th event the UKS plasma instrument shows that the solar wind velocity decreases by about 50 km/sec near the upstream edge of the cloud [Coates et al., 1985]. The September 11th event shows a similar decrease in the solar wind velocity. Third, to qualify as a shock the entropy must increase as the plasma flows across the discontinuity. Wave-particle interactions caused by the intense electric field noise upstream of the ion cloud certainly could cause an increase in entropy. However, the entropy production cannot be verified directly because the plasma instrument does not have sufficient space and time resolution to accurately determine the temperature and density variations in the region where the noise is observed.

The above considerations support the view that the noise upstream of the ion cloud could be associated with a shock, but do not prove that it is a shock. If it is a shock, then it cannot be a conventional magnetohydrodynamic (MHD) shock. For a MHD shock the ion cyclotron radii must be small compared to the radius of curvature of the discontinuity, otherwise magnetohydrodynamics would not apply. From relatively simple pressure balance considerations Haerendel et al. [1985] estimate that the radius of the diamagnetic cavity is about 30 km. For a representative solar wind ion temperature of 10^5°K and a magnetic field strength of 8nT it can be shown that the

quite striking. In both cases the noise is almost completely electrostatic and extends over a broad range of frequencies, from a few Hz to several kHz. An electric field spectrum of the noise observed in the earth's bow shock is shown in Figure 6. This spectrum is from the time of maximum intensity at 0251:20 UT. The similarity of this spectrum to the spectrums in Figures 3 and 4 is clearly evident. In both cases the noise extends with relatively high intensities from a few Hz to a few kHz, and then decreases rapidly with increasing frequency. As in the case of the noise upstream of the artificial ion cloud, the detailed shape of the spectrum in the bow shock varies somewhat from event to event. In some cases the spectrum has a peak at a frequency of a few hundred Hz, similar to the example in Figure 4, whereas in other cases it is nearly flat, as in Figure 6. Wideband spectrums show that the noise in the bow shock is very impulsive and usually does not have a detectable spin modulation, very similar to the noise observed upstream of the artificial ion cloud. For a survey of representative spectrums of the electric field noise in the earth's bow shock, see Rodriguez and Gurnett [1975]. Although the overall features are similar, the noise associated with the artificial ion cloud is more intense than the noise in the bow shock, typically by a factor of ten to one hundred.

To interpret the effects upstream of the ion cloud as a shock certain basic conditions must be satisfied. First, the plasma must have a component of flow normal to the surface of the discontinuity. This condition is known to be satisfied since the plasma instrument

III. IS THE ELECTROSTATIC NOISE ASSOCIATED WITH A SHOCK?

The location of the intense electrostatic noise upstream of the ion cloud raises the question as to whether this noise is associated with a shock. For many years it has been known that an intense burst of electrostatic noise is present in the earth's bow shock [Fredricks et al., 1968, 1970a,b; Rodriguez and Gurnett, 1975]. It is now widely believed that in a collisionless plasma this noise causes heating and dissipation very similar to collisions in an ordinary gas-dynamic shock. The close similarity of the electrostatic noise to the noise in the earth's bow shock is illustrated in Figure 5, which shows a crossing of the earth's bow shock by the ISEE 1 spacecraft on November 7, 1977. The top panel of Figure 5 shows the electric field intensities and the bottom three panels, from Paschmann et al. [1982], show the electron density N_e, the reflected ion density, N_I, and the magnetic field strength, B. The shock can be identified by the abrupt increase in the electron density and magnetic field strength from about 2250:55 to 2251:20 UT. This region of rapidly increasing plasma density and magnetic field strength is called the transition region. The top panel of Figure 5 shows that an intense burst of electric field noise is present in the transition region.

The similarities between the electric field noise upstream of the artificial ion cloud and the noise in the earth's bow shock are

realistic parameters it is found that the ion beam-plasma instability occurs for a range of lithium-to-proton density ratios between about 2.5×10^{-2} and 50. These limits explain why the noise only occurs near the outer edge of the ion cloud, in the region where the lithium-to-proton density ratio is near unity. The maximum growth rates increase if cold electrons associated with the lithium photoionization are present in the plasma. Currents do not play an important role in generating the noise.

At present the importance of the electrostatic noise has not been established. The noise is very intense and occurs in a region of elevated electron temperatures. Although the main electron energization is thought to be caused by adiabatic acceleration in the magnetic field upstream of the cloud [Paschmann et al., 1985], the noise may play a role in the pitch-angle scattering and diffusion of these electrons. If the noise is associated with an electrostatic shock, then the turbulent electric fields probably play an important role in the ion heating and dissipation in the shock. Since the phase velocity of the unstable waves is near the lithium thermal velocity, the turbulence should be very effective at heating the lithium ions.

It is likely that the intense electrostatic noise observed during the AMPTE ion releases is closely related to a variety of other situations where intense electric field noise is produced by a neutral gas interacting with a rapidly moving plasma. These situations include (1) intense electric field noise associated with cesium ion release in the earth's ionosphere [Kintner et al., 1980],

(2) intense electrostatic noise observed in the vicinity of the Space Shuttle [Shawhan and Murphy, 1983], apparently caused by an interaction of gases from the Shuttle with the surrounding ionosphere, and (3) electric field noise observed by Voyager 1 in the vicinity of Titan [Gurnett et al., 1981]. Because of the close similarity of the lithium releases to the gaseous envelope around a comet, it will be interesting to see if a comparable type of noise is observed during the forthcoming fly-bys of the comets Giacobini-Zinner and Halley.

ACKNOWLEDGEMENTS

The research at the University of Iowa was supported by the Office of Naval Research through contract N00014-82-K-0183 and grant N00014-76-C-0016, and by the National Aeronautics and Space Administration through grants NGL-16-001-002 and NGL-16-001-043, and contract NAS5-28701. The research at The Aerospace Corporation was supported in part by ONR and in part by the U.S. Air Force System Command Space Division under contract F04701-84-C-0085. The research at the University of Washington was supported by ONR Contract N00014-84-K-0160.

REFERENCES

Anderson, R. R., D. A. Gurnett, B. Häusler, H. C. Koons, R. H. Holzworth, R. A. Treumann, O. H. Bauer, G. Haerendel, H. Lühr, L. J. Woolliscroft, and M. P. Gough, Electron number density from the AMPTE/IRM plasma wave experiment during solar wind lithium releases, J. Geophys. Res., submitted, 1985.

Coates, A. J., A. D. Johnstone, M. F. Smith, and D. J. Rodgers, AMPTE-UKS Ion experiment observations of lithium releases in the solar wind, J. Geophys. Res., this issue, 1985.

Forslund, D. W., and C. R. Shonk, Formation and structure of electrostatic collisionless shocks, Phys. Rev. Lett., 25, 1699, 1970.

Fredricks, R. W., F. W. Coroniti, C. F. Kennel and F. L. Scarf, Fast-resolved spectra of electrostatic turbulence in the earth's bow shock, Phys. Rev. Lett., 24, 994, 1970a.

Fredricks, R. W., G. M. Crook, C. F. Kennel, I. W. Green, and F. L. Scarf, OGO 5 observations of electrostatic turbulence in bow shock magnetic structures, J. Geophys. Res., 75, 3751, 1970b.

Fredricks, R. W., C. F. Kennel, F. L. Scarf, G. M. Crook, and I. M. Green, Detection of electric-field turbulence in the earth's bow shock, Phys. Rev. Lett., 21, 1761, 1968.

Fried, B. D., and S. D. Conte, The Plasma Dispersion Function, Academic Press, N. York, 1961.

Fried, B., and A. Y. Wong, Stability limits for longitudinal waves in ion beam-plasma interactions, Phys. Fluids, 9, 1084, 1966.

Gurnett, D. A., Waves and instabilities associated with collisionless shocks, Collisionless Shock Waves in the Heliosphere, ed. by R. Stone and B. Tsurutani, AGU, Washington, DC, 1984.

Gurnett, D. A., W. S. Kurth, and F. L. Scarf, Plasma waves near Saturn: Initial results from Voyager 1, Science, 212, 239, 1981.

Haerendel, G., Plasma confinement and interaction experiment, Active Experiments in Space, ESA Report SP-196, 337, 1983.

Haerendel, G., Interaction of lithium clouds with the interplanetary medium, J. Geophys. Res., this issue, 1985.

Haerendel, G., A. Valenzuela, H. Föppl, B. Häusler, F. Melzner, G. Paschmann, and J. Stöcker, Physical properties of the lithium injection experiments in the solar wind, J. Geophys. Res., this issue, 1985.

Häusler, B., R. R. Anderson, D. A. Gurnett, H. C. Koons, R. H. Holtzworth, O. H. Bauer, R. Treuman, K. Gnaiger, D. Odem, W. B. Harbridge, and F. Eberl, The plasma wave instrument onboard the AMPTE-IRM spacecraft, IEEE Trans. Geosci. Electronics, submitted for publication, 1985a.

Häusler, B., R. H. Holzworth, L. J. Woollischroft, R. R. Anderson, D. A. Gurnett, H. C. Koons, O. H. Bauer, G. Haerendel, A. G. Darbyshire, M. P. Gough, S. R. Jones, N. Klöcker, A. J. Norris, G. Paschmann, and A. Valenzuela, Plasma waves observed by the IRM and UKS spacecraft during the AMPTE solar wind lithium releases: Overview, J. Geophys. Res., this issue, 1985b.

Hundhausen, A. J., Coronal Expansion and Solar Wind, Springer-Verlag, N. York, 44, 1972.

Ikezi, H., T. Kamimura, M. Kada, and K. E. Lonngren, Laminar electrostatic shock waves generated by an ion-beam, Phys. Fluids, 16, 2304, 1973.

Imre, K., and E. Özizmir, Comments on "Stability limits for longitudinal waves in ion beam-plasma interactions," Phys. Fluids, 17, 1046, 1974.

Kintner, P. M., M. C. Kelley, G. Holmgren, and R. Bostrom, The observation and production of ion acoustic waves during the trigger experiment, J. Geophys. Res., 85, 5071, 1980.

Krimigis, S. M., G. Haerendel, R. W. McEntire, G. Paschmann, and D. A. Bryant, The Active Magnetostpheric Particle Tracer Explorers (AMPTE) Program, EOS, 63, 843, 1982.

Krall, N. A., and A. W. Trivelpiece, Principles of Plasma Physics, McGraw-Hill, N. York, 473, 1973.

Means, R., F. Coroniti, A. Wong, and R. White, Turbulence in electrostatic ion-acoustic shocks, Phys. Fluids, 16, 2304, 1973.

Montgomery, D., and G. Joyce, Shock-like solutions of the electrostatic Vlasov equation, J. Plasma Phys., 3, 1, 1969.

Muller, D. E., A method for solving algebraic equations using an automatic computer, Math. Comp., 10, 208, 1956.

Paschmann, G., N. Sckopke, S. J. Bame, and J. T. Gosling, Observations of gyrating ions in the foot of the nearly perpendicular shock, Geophys. Res. Lett., 9, 881, 1982.

Paschmann, G., C. W. Carlson, W. Baumjohann, D. W. Curtis, N. Sckopke, and G. Haerendel, Plasma observations on AMPTE-IRM for the Li-Releases in the solar wind, J. Geophys. Res., this issue, 1985.

Rodriguez, P., and D. A. Gurnett, Electrostatic and electromagnetic turbulence associated with the earth's bow shock, J. Geophys. Res., 80, 19, 1975.

Shawhan, S. D., and G. B. Murphy, Plasma diagnostics package assessment of the STS-3 orbiter plasma environment, J. Spacecraft and Rockets, Special STS-31055-1 issue, 1983.

Tidman, D. A., and N. A. Krall, Shock Waves in Collisionless Plasmas, John Wiley, N. York, 1971.

FIGURE CAPTIONS

Figure 1 — A summary of the plasma density, magnetic field, and electric field observations for the September 20, 1984, solar wind lithium release. Note the intense burst of electrostatic noise from about 19 to 28 seconds after the injection, as the magnetic field returns to the upstream value. A somewhat similar burst of noise was observed following the September 11, 1984, lithium release.

Figure 2 — A schematic illustration showing the inferred plasma and magnetic field configuration associated with the September solar wind ion releases. The intense burst of electrostatic noise is observed on the upstream edge of the region of draped magnetic field lines.

Figure 3 — The peak and average electric field spectrums for the September 20th event. The peak spectrum shows that the maximum electric field intensities occurred in the frequency range around a few hundred Hz. The intensities decrease rapidly at frequencies above a few kHz.

Figure 4 The peak and average electric field spectrums for the September 11th event. Again, the peak electric field intensities are in the region around one hundred Hz, with significant noise intensities extending up to a few kHz.

Figure 5 The plasma density, magnetic field, and electric field measurements for a crossing of the earth's bow shock by the ISEE-1 spacecraft on November 7, 1977. The electrostatic noise observed on this and other shock crossings is very similar to the noise observed upstream of the AMPTE artificial ion clouds.

Figure 6 The electric field spectrum at the time of maximum intensity for the shock crossing in Figure 5. Note the very close similarity to the artificial ion cloud spectrums in Figures 3 and 4.

Figure 7 A schematic representation of the ion distribution function in the vicinity of the artificial ion cloud. The lithium ions are born essentially at rest in the spacecraft frame of reference. The solar wind protons stream essentially uninhibited through the ion cloud with a velocity V_{sw}. This double-humped distribution is known to be highly unstable.

Figure 8 A model for the cold electron distribution in which the cold and hot electrons both drift at a velocity, V_D, that is determined by the $\vec{v} \times \vec{B}$ electric field. This model applies mainly to the motion perpendicular to the magnetic field.

Figure 9 Plots of the growth rate, γ, and normalized wave number, $k\lambda_D$, as a function of frequency for the instability associated with the minimum of F(v) between 0 and V_D. The solid lines are for $N_e^c = 0$, and the dashed lines are for $N_e^c = N_{Li}$.

Figure 10 The frequencies of marginal stability, $\gamma = 0$, and maximum growth rate, γ_{max}, as a function of the lithium to proton density ratio, N_{Li}/N_p. This case is for $N_e^c = 0$. Note the limited range of N_{Li}/N_p over which instability occurs. Also, note that the maximum frequency of the instability compares favorably with the observed frequency range of the noise in Figures 3 and 4.

Figure 11 The frequencies of marginal stability, $\gamma = 0$, and maximum growth rate, γ_{max}, as a function of the lithium to proton density ratio, N_{Li}/N_p. This case is for $N_e^c = N_{Li}$.

Figure 12 The maximum growth rate of the ion beam-plasma instability as a function of the lithium to proton density ratio. Note that the highest growth rate occurs when $N_{Li} = N_p$. This result also agrees with the observations in Figure 1, which show that the most intense noise occurs at about the time that $N_{Li} \simeq N_p$.

Figure 13 Marginal instability boundaries comparable to Figure 13 showing the effect of a current. The cross-hatched region shows the variation in the $\gamma = 0$ boundary for a ±25% variation in the electron drift velocity. These limits represent the maximum variations that could be produced by the currents in the upstream boundary region.

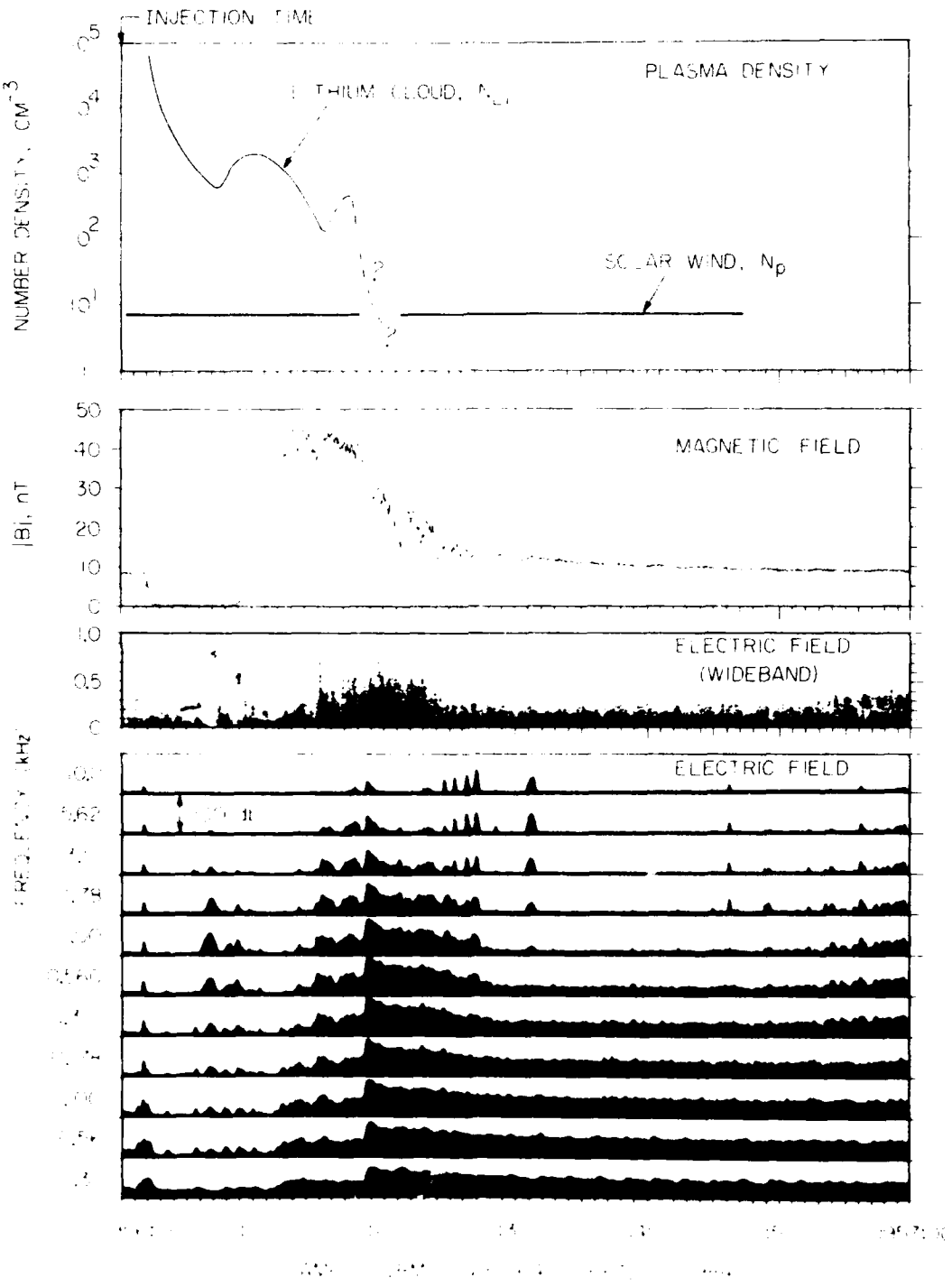
INJECTION TIME
PLASMA DENSITY
THRIUM CLOUD, N_{Li}
SOLAR WIND, N_p
NUMBER DENSITY, CM^{-3}
MAGNETIC FIELD
|B|, nT
ELECTRIC FIELD
(WIDEBAND)
ELECTRIC FIELD

Figure 1

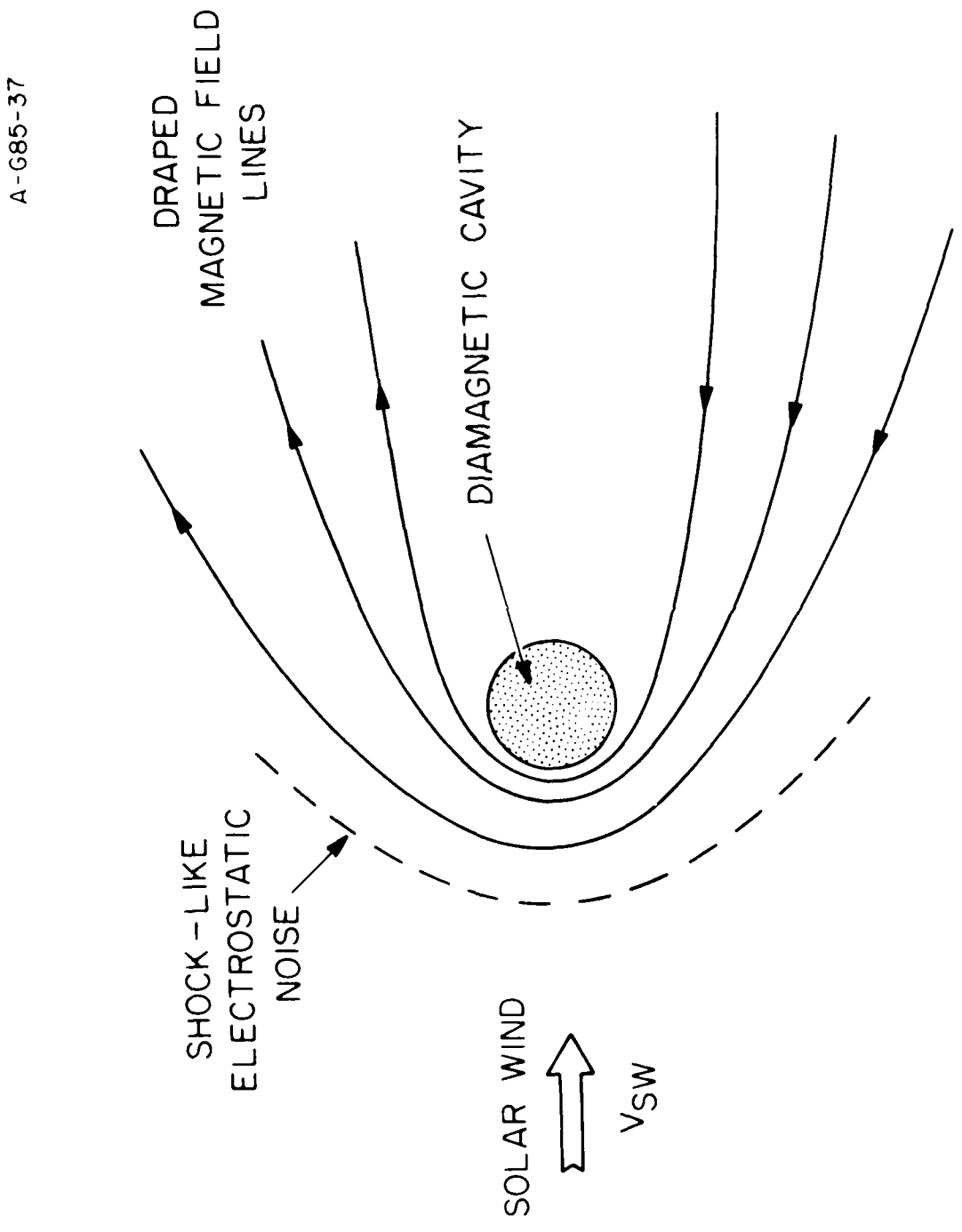
A-G85-37
DRAPED
MAGNETIC FIELD
LINES
DIAMAGNETIC CAVITY
SHOCK-LIKE
ELECTROSTATIC
NOISE
SOLAR WIND
V_{SW}

Figure 2

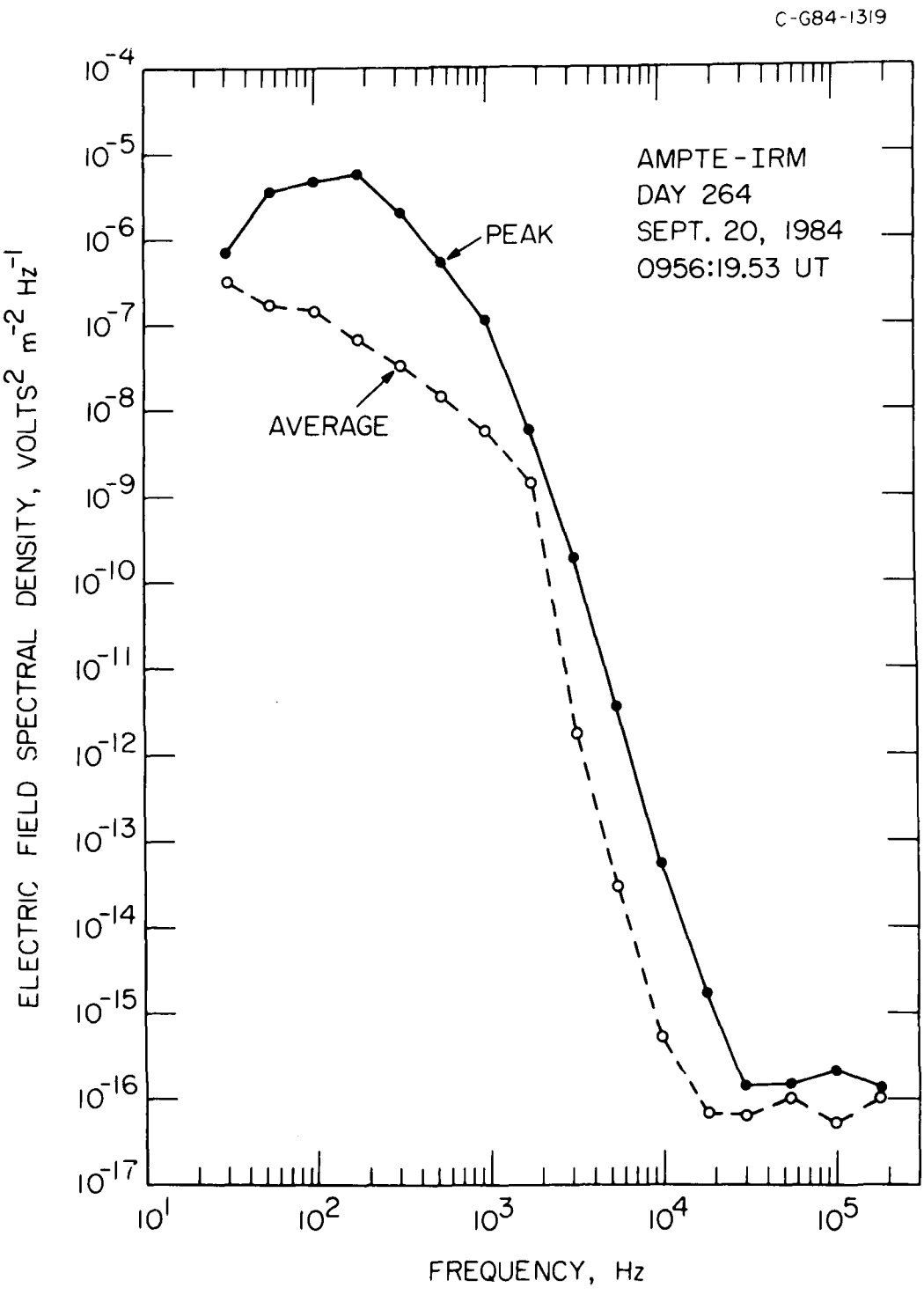
C-G84-1319
AMPTE-IRM
DAY 264
SEPT. 20, 1984
0956:19.53 UT
PEAK
AVERAGE
ELECTRIC FIELD SPECTRAL DENSITY, VOLTS^2 m^{-2} Hz^{-1}
FREQUENCY, Hz
10^{-4}
10^{-5}
10^{-6}
10^{-7}
10^{-8}
10^{-9}
10^{-10}
10^{-11}
10^{-12}
10^{-13}
10^{-14}
10^{-15}
10^{-16}
10^{-17}
10^{1}
10^{2}
10^{3}
10^{4}
10^{5}

Figure 3

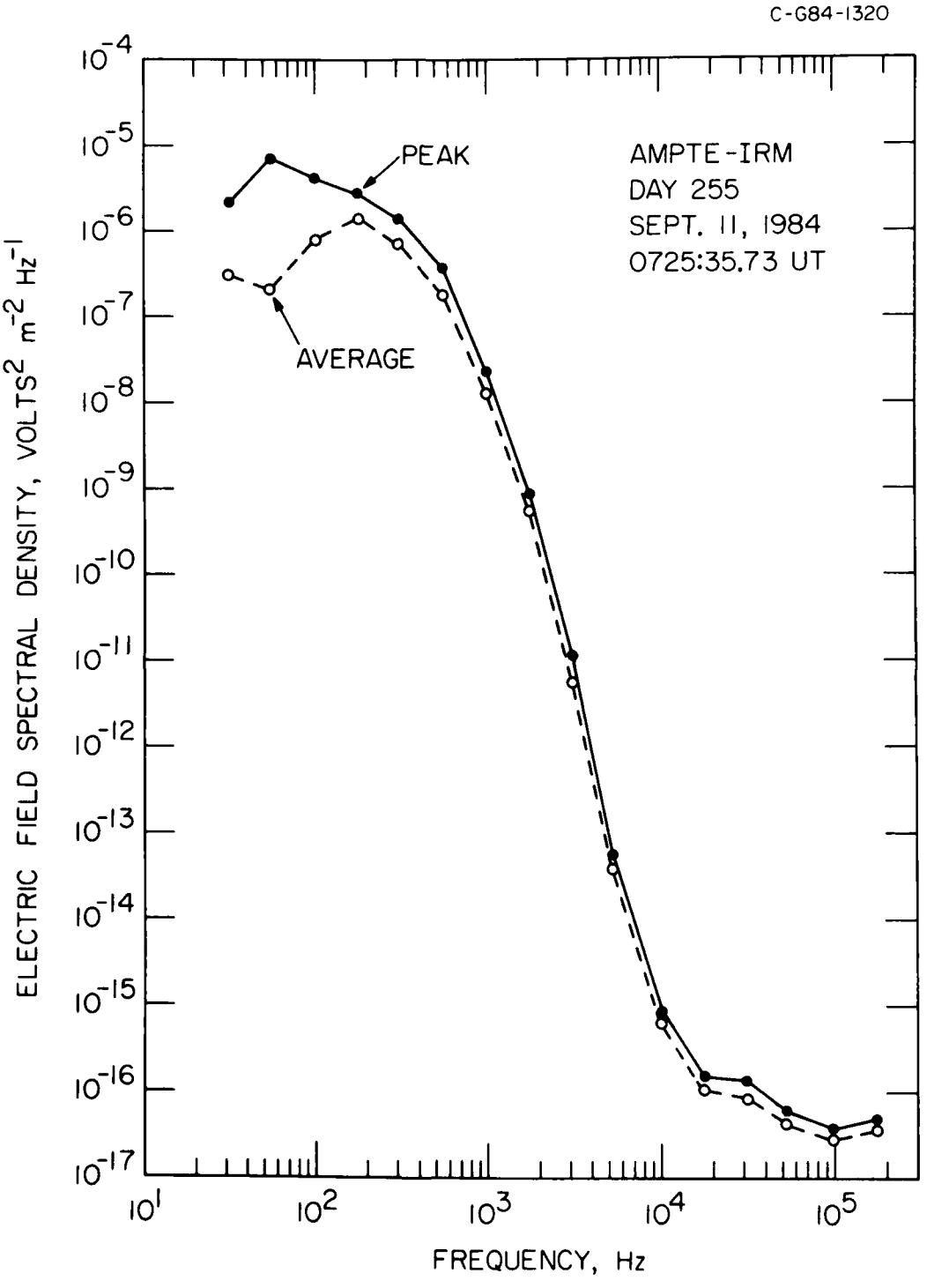
C-G84-1320
PEAK
AVERAGE
AMPTE-IRM
DAY 255
SEPT. 11, 1984
0725:35.73 UT
ELECTRIC FIELD SPECTRAL DENSITY, VOLTS^2 m^{-2} Hz^{-1}
FREQUENCY, Hz
10^{-4}
10^{-5}
10^{-6}
10^{-7}
10^{-8}
10^{-9}
10^{-10}
10^{-11}
10^{-12}
10^{-13}
10^{-14}
10^{-15}
10^{-16}
10^{-17}
10^{1}
10^{2}
10^{3}
10^{4}
10^{5}

Figure 4

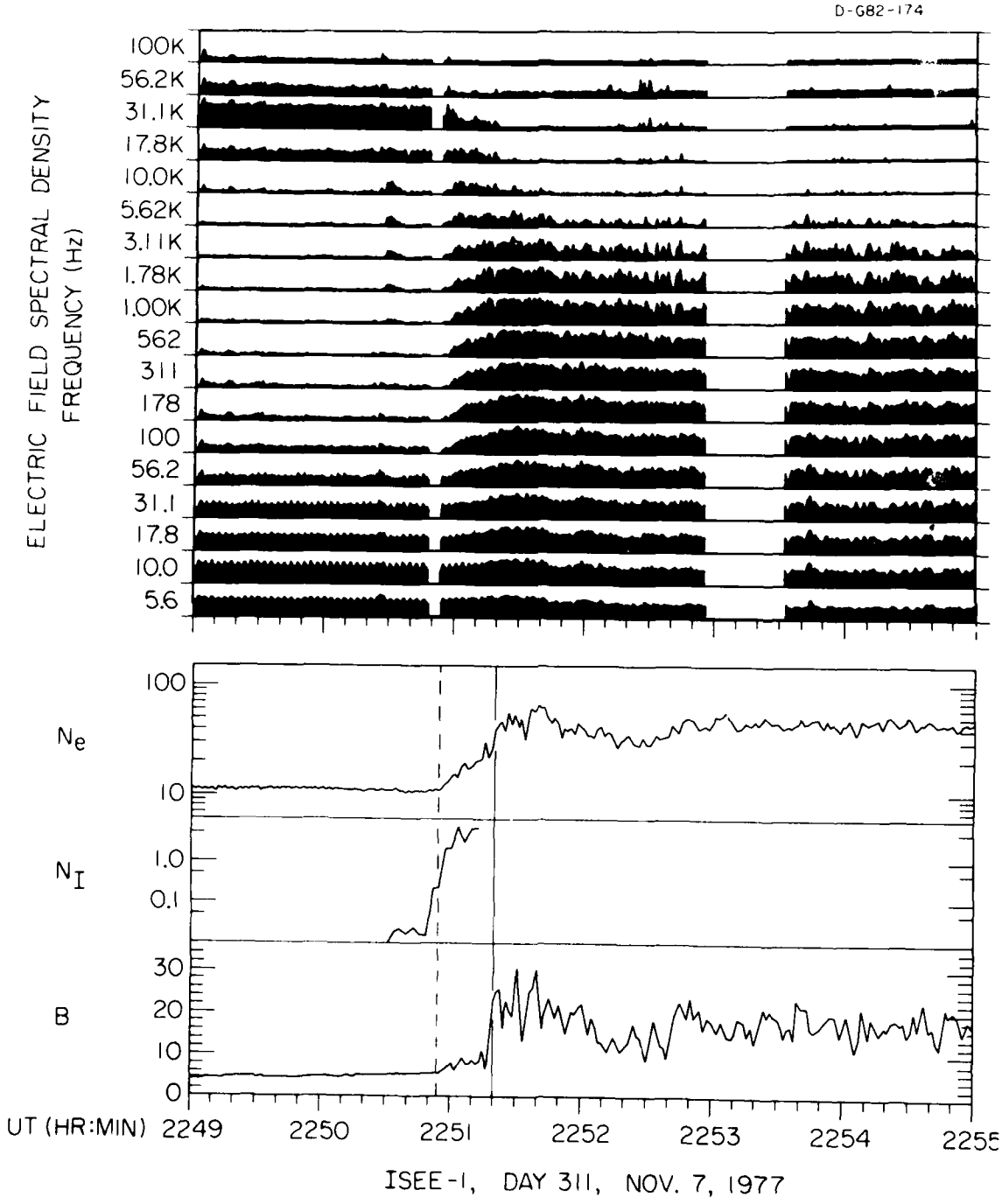
D-G82-174
ELECTRIC FIELD SPECTRAL DENSITY
FREQUENCY (Hz)
100K
56.2K
31.1K
17.8K
10.0K
5.62K
3.11K
1.78K
1.00K
562
311
178
100
56.2
31.1
17.8
10.0
5.6
Ne
100
10
NI
1.0
0.1
B
30
20
10
0
UT (HR:MIN) 2249
2250
2251
2252
2253
2254
2255
ISEE-1, DAY 311, NOV. 7, 1977

Figure 5

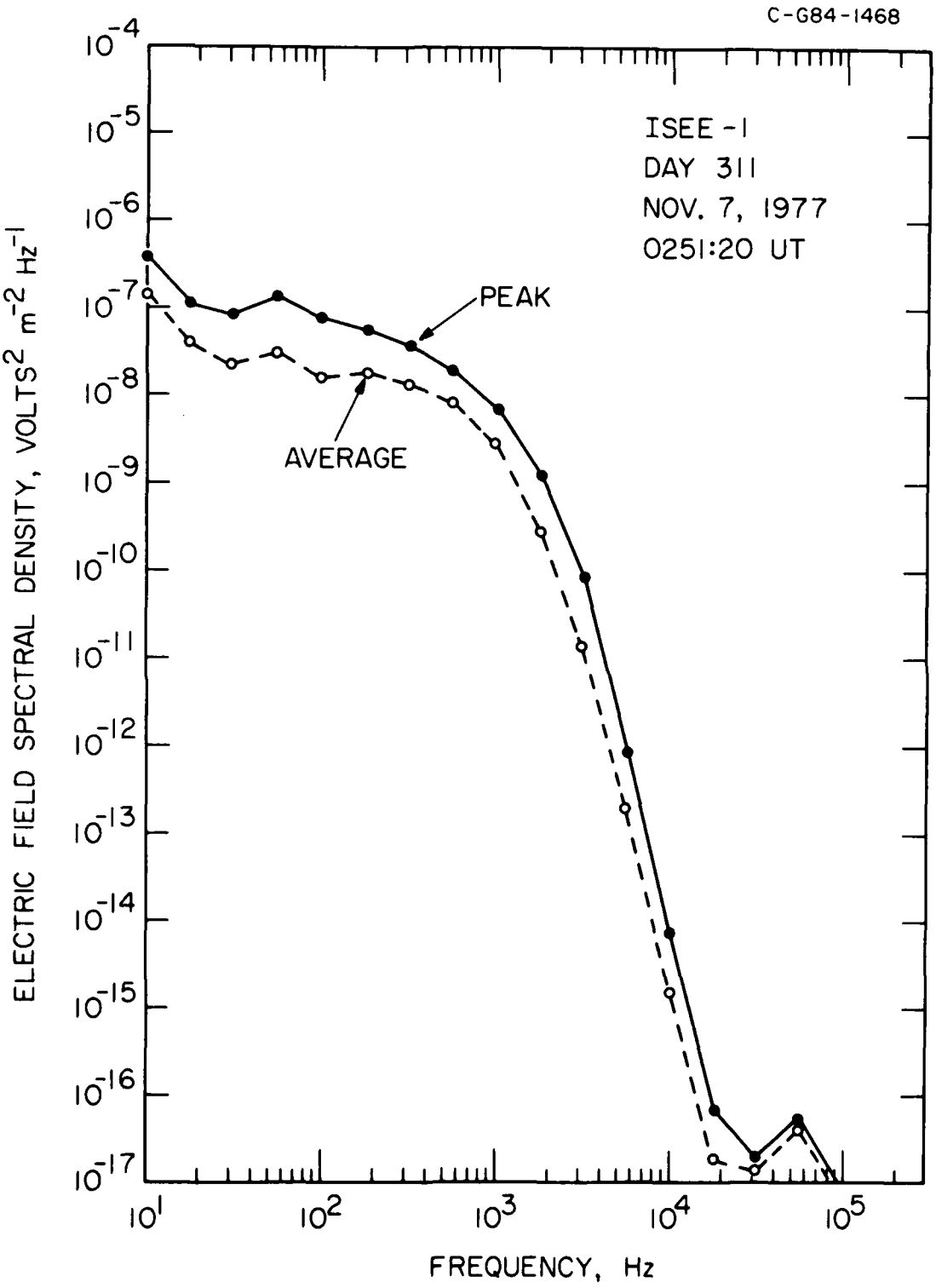
C-G84-1468
ISEE-1
DAY 311
NOV. 7, 1977
0251:20 UT
PEAK
AVERAGE
ELECTRIC FIELD SPECTRAL DENSITY, VOLTS^2 m^{-2} Hz^{-1}
FREQUENCY, Hz
10^{-4}
10^{-5}
10^{-6}
10^{-7}
10^{-8}
10^{-9}
10^{-10}
10^{-11}
10^{-12}
10^{-13}
10^{-14}
10^{-15}
10^{-16}
10^{-17}
10^{1}
10^{2}
10^{3}
10^{4}
10^{5}

Figure 6

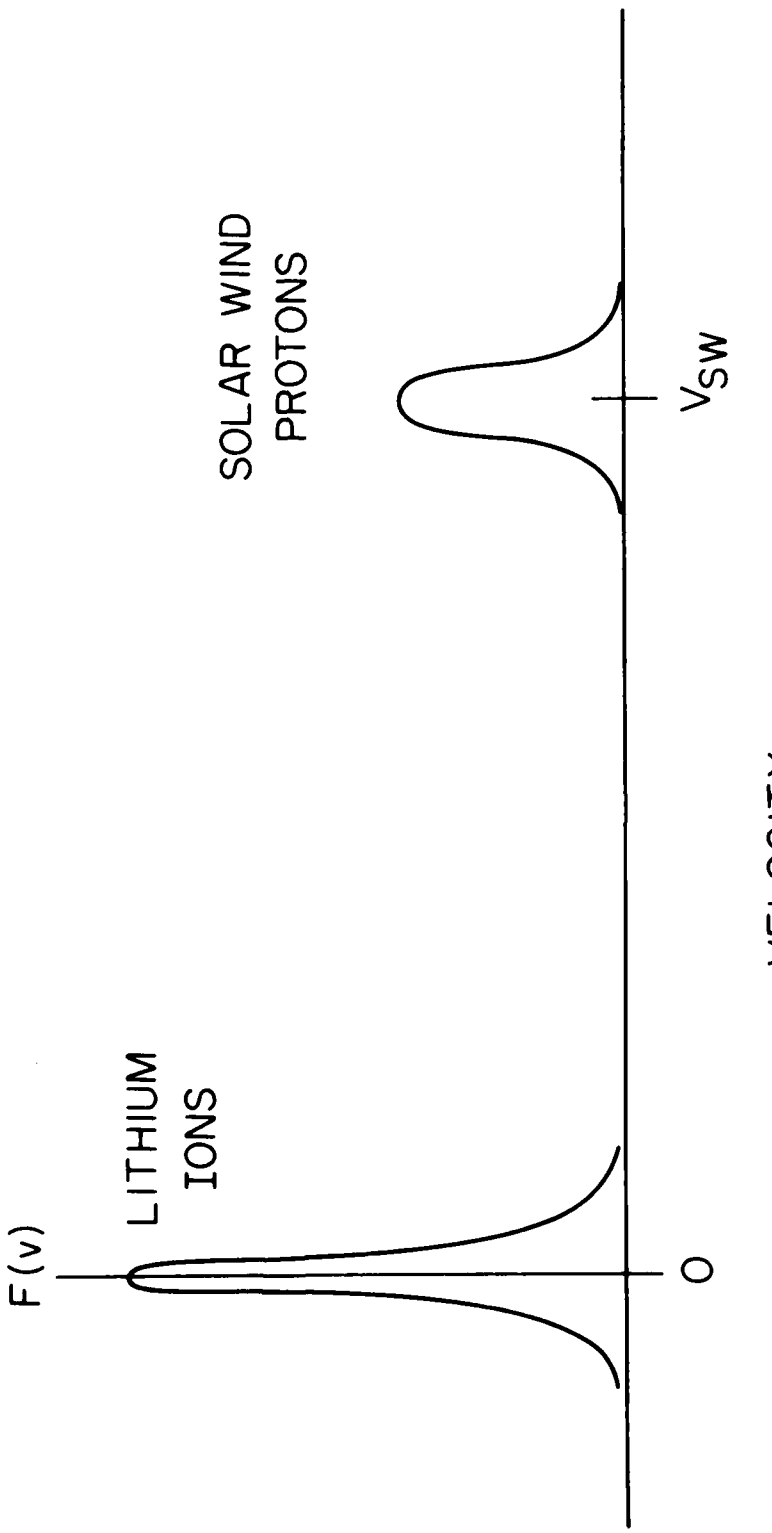

Figure 7

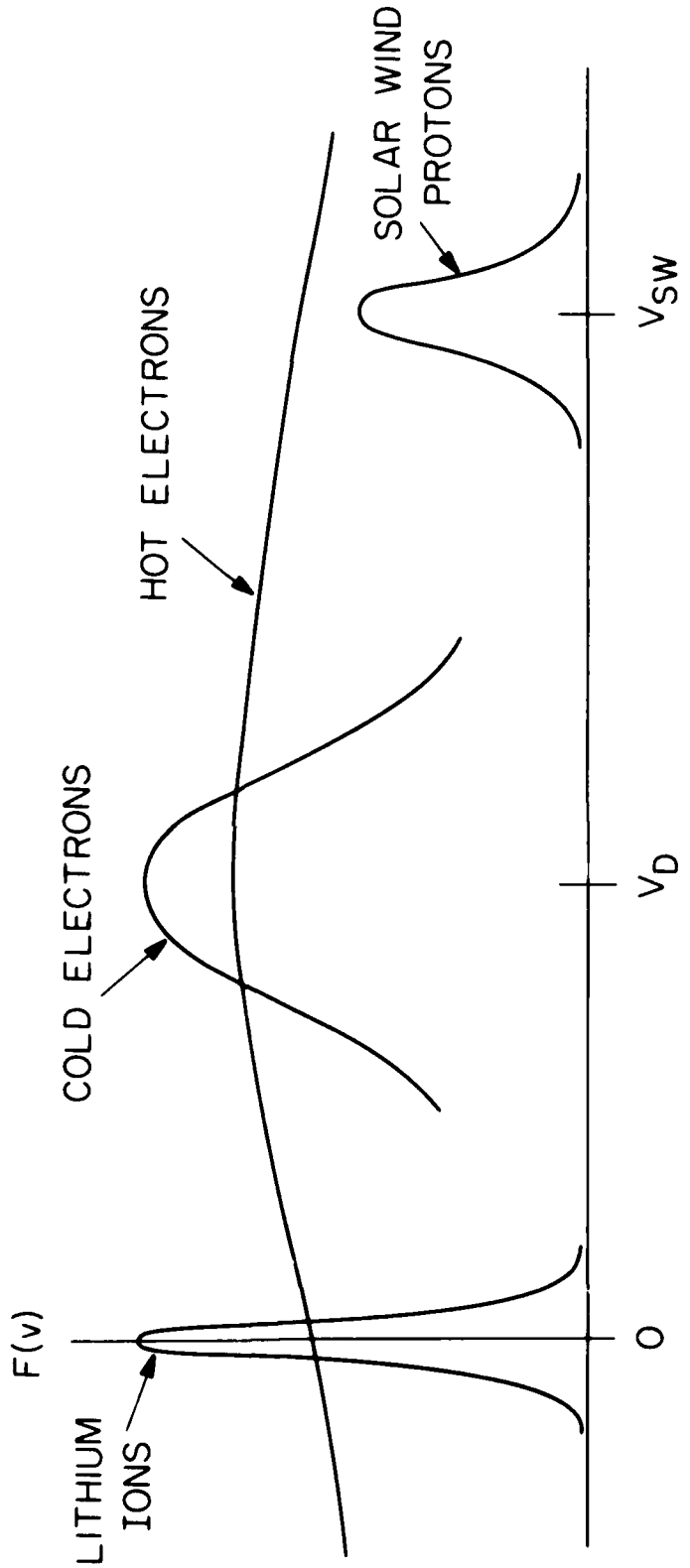
B-G85-65
F(v)
LITHIUM IONS
COLD ELECTRONS
HOT ELECTRONS
SOLAR WIND PROTONS
0
V_D
V_{SW}
VELOCITY

Figure 8

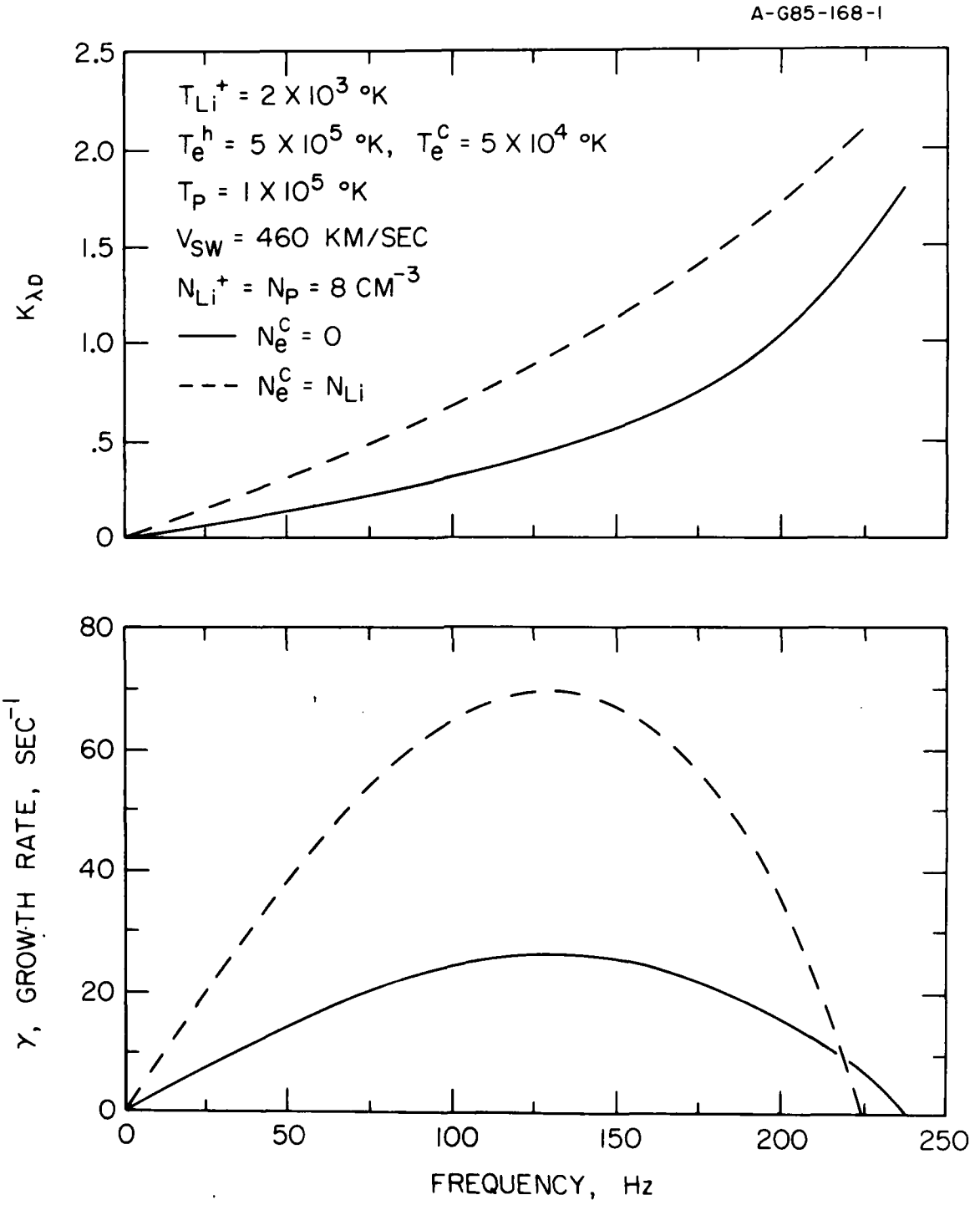
A-G85-168-1
$T_{Li}^{+} = 2 \times 10^3$ °K
$T_e^h = 5 \times 10^5$ °K, $T_e^c = 5 \times 10^4$ °K
$T_p = 1 \times 10^5$ °K
V_{SW} = 460 KM/SEC
$N_{Li}^{+} = N_p = 8$ CM^{-3}
$N_e^c = 0$
$N_e^c = N_{Li}$
$K_{\lambda D}$
2.5
2.0
1.5
1.0
.5
0
80
60
40
20
0
50
100
150
200
250
γ, GROWTH RATE, SEC^{-1}
FREQUENCY, Hz

Figure 9

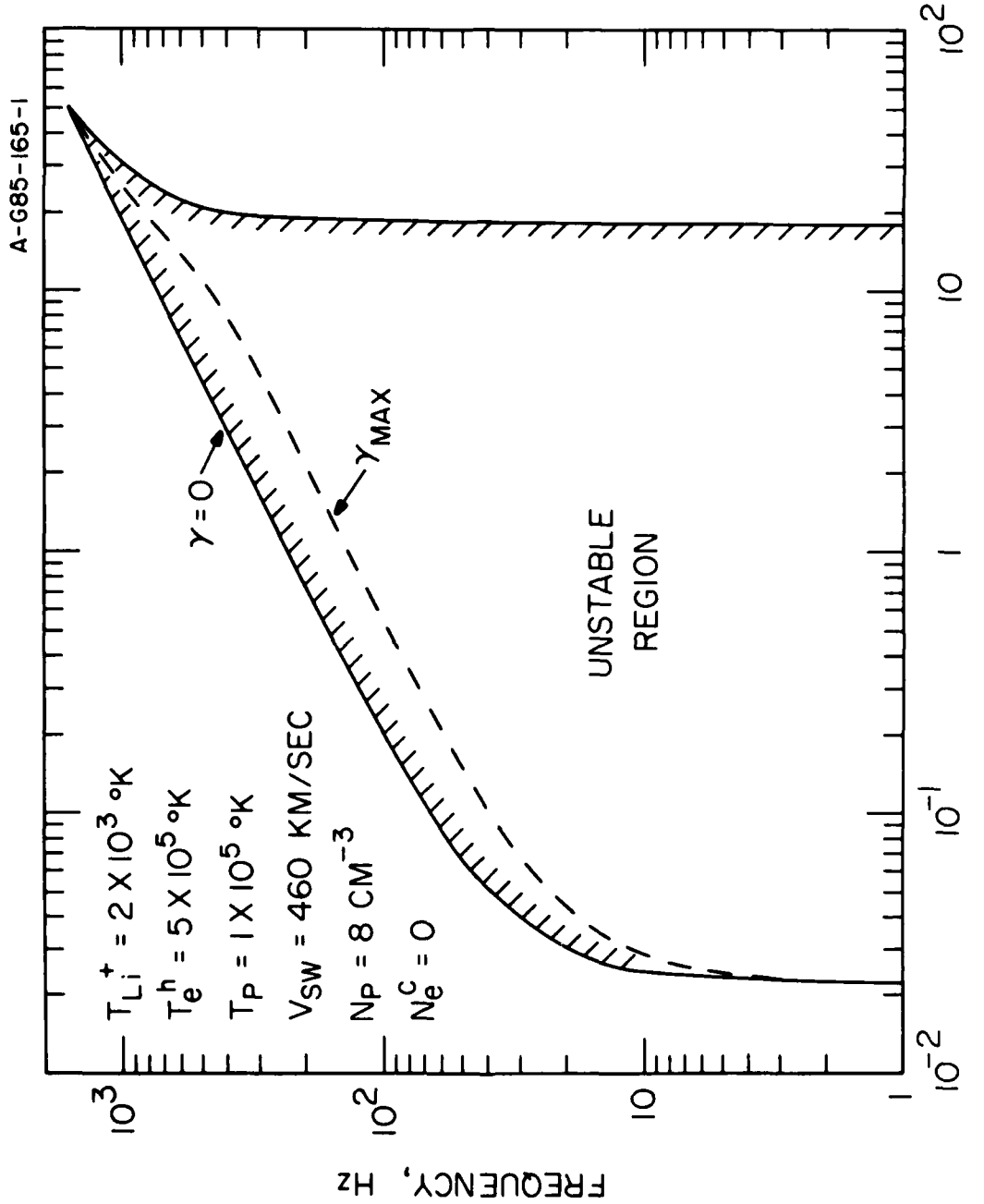
A-685-165-1
$T_{Li}^{+} = 2 \times 10^3$ °K
$T_e^h = 5 \times 10^5$ °K
$T_P = 1 \times 10^5$ °K
$V_{SW} = 460$ KM/SEC
$N_P = 8$ CM^{-3}
$N_e^c = 0$
$\gamma = 0$
γ_{MAX}
UNSTABLE REGION
FREQUENCY, Hz
10^3
10^2
10
1
10^{-2}
10^{-1}
1
10
10^2
N_{Li}^{+}/N_P, LITHIUM TO PROTON DENSITY RATIO

Figure 10

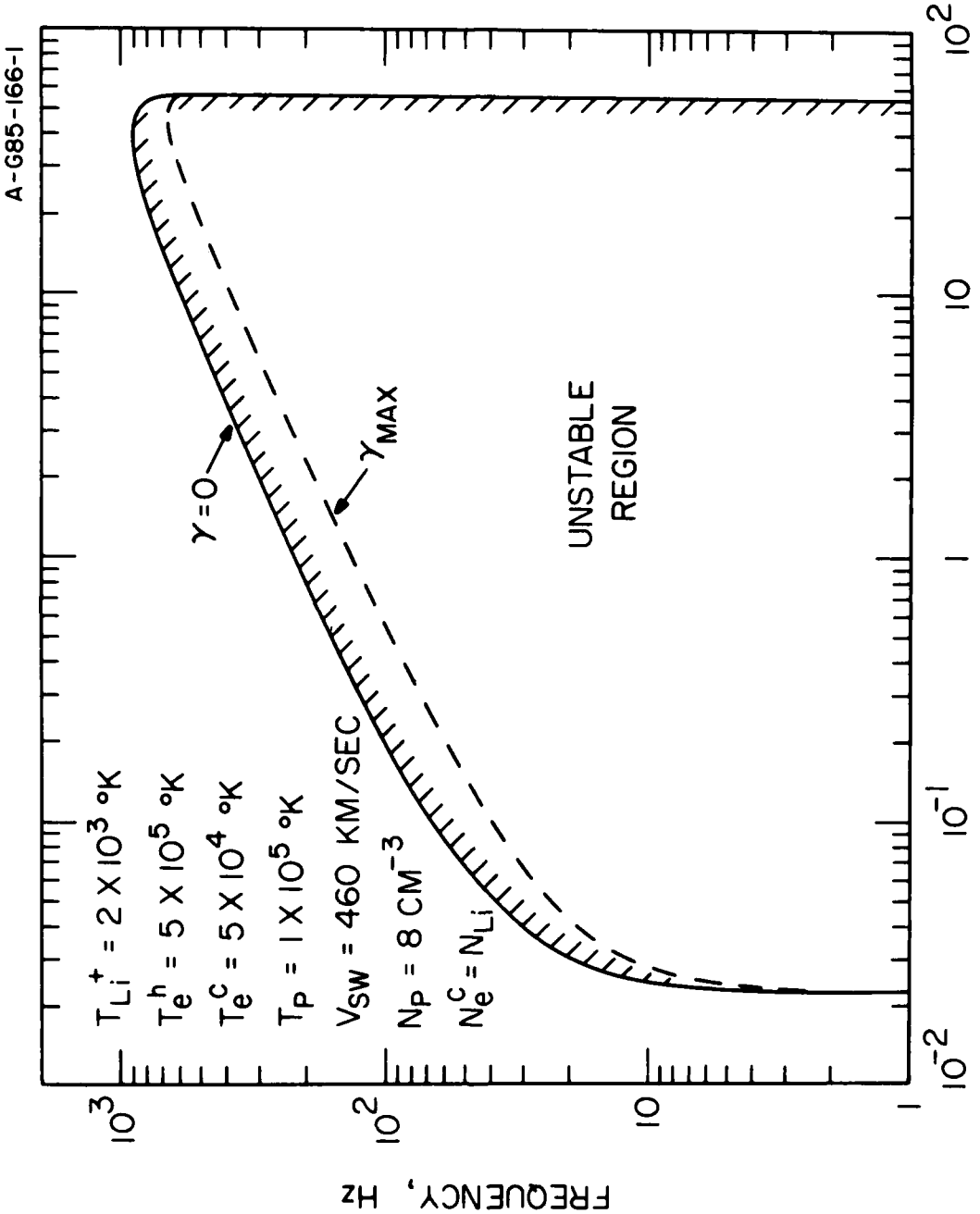
A-G85-166-1
FREQUENCY, Hz
10^3
10^2
10
1
10^{-2}
10^{-1}
1
10
10^2
N_{Li}^+/N_P, LITHIUM TO PROTON DENSITY RATIO
UNSTABLE REGION
γ_{MAX}
$\gamma=0$
$T_{Li}^+ = 2 \times 10^3$ °K
$T_e^h = 5 \times 10^5$ °K
$T_e^c = 5 \times 10^4$ °K
$T_P = 1 \times 10^5$ °K
V_{SW} = 460 KM/SEC
N_P = 8 CM^{-3}
$N_e^c = N_{Li}$

Figure 11

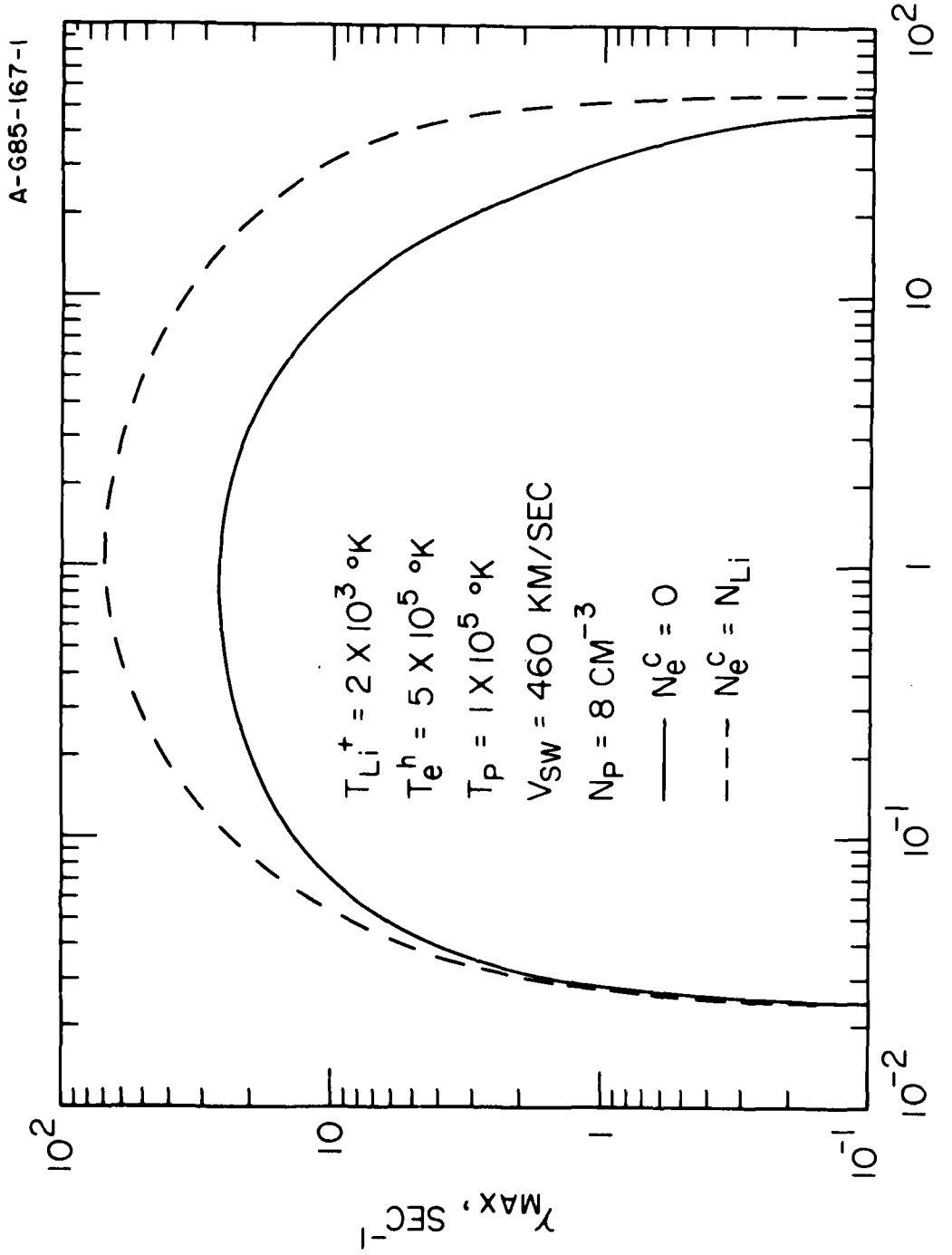
A-685-167-1
γ_{MAX}, SEC^{-1}
10^2
10
1
10^{-1}
10^{-2}
10^2
10
1
10^{-1}
N_{Li}^+/N_P, LITHIUM TO PROTON DENSITY RATIO
$T_{Li}^+ = 2 \times 10^3$ °K
$T_e^h = 5 \times 10^5$ °K
$T_P = 1 \times 10^5$ °K
$V_{SW} = 460$ KM/SEC
$N_P = 8$ CM^{-3}
$N_e^c = 0$
$N_e^c = N_{Li}$

Figure 12

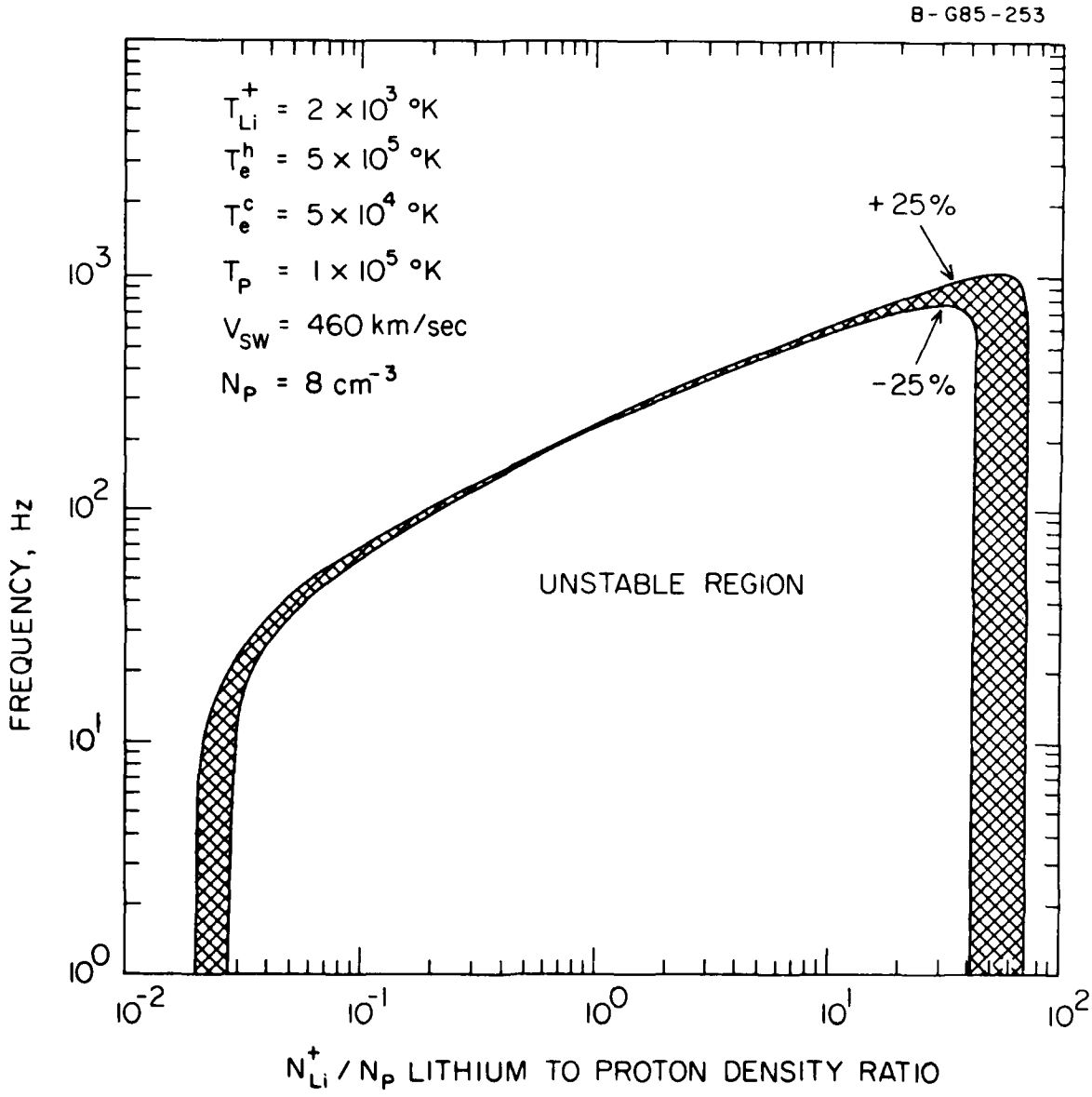
B-G85-253
T_{Li}^{+} = 2 × 10³ °K
T_e^h = 5 × 10⁵ °K
T_e^c = 5 × 10⁴ °K
T_P = 1 × 10⁵ °K
V_{SW} = 460 km/sec
N_P = 8 cm⁻³
+25%
-25%
UNSTABLE REGION
FREQUENCY, Hz
10³
10²
10¹
10⁰
10⁻²
10⁻¹
10⁰
10¹
10²
N_{Li}^{+} / N_P LITHIUM TO PROTON DENSITY RATIO

Figure 13

END

FILMED

9-85

DTIC